AIMS Mathematics, 11(3): 6777–6803.
DOI: 10.3934/math.2026280
Received: 16 November 2025
Revised: 17 February 2026
Accepted: 27 February 2026
Published: 16 March 2026

https://www.aimspress.com/journal/Math

Research article

Physics-informed weighted Ramos–Louzada model: integrating statistical and physical constraints for survival analysis

Mashail M. AL Sobhi*

Department of Mathematics, Umm-Al-Qura University, Makkah 24227, Saudi Arabia

* **Correspondence:** mashail1426@gmail.com.

Abstract: The paper proposes a new physics-informed, weighted length-biased Ramos–Louzada (WLBRL) system for survival and reliability analysis, combining statistical inference with physical constraints. The suggested WLBRL distribution explicitly corrects for length-biased sampling, and physics-informed neural networks (PINNs) impose relationships on survival hazards in estimation that are implicitly defined by differential equations. The physics-informed maximum likelihood estimation approach is presented to stabilize parameter inference under noisy, limited data. Vast simulation literature and real-world medical and engineering data have shown that the proposed framework reduces mean squared error by 40% compared to the classical Ramos–Louzada (RL), Weibull, and exponential models. These findings verify that integrating physical laws into weighted survival models enhances estimation accuracy, robustness, and explainability, indicating that the weighted length-biased Ramos–Louzada physics-informed neural network (WLBRL-PINN) system is generally applicable to uncertainty-aware risk assessment in biomedical and engineering systems.

Keywords: weighted Ramous–Louzada distribution; physics-informed neural network; parameter estimation; simulation study
Mathematics Subject Classification: 62N01, 62F10

1. Introduction

Research on probabilistic models has seen growing interest in survival analysis and reliability theory, as weighted [1] and length-biased distributions [2] have become increasingly relevant to these fields. The Ramos–Louzada (RL) distribution has been modified to better address real-world biases

and uncertainties in its application. Scientists now employ the physics-informed systems (PIS) approach to improve predictive power by combining differential equations with data-driven methods. Applying physics-informed neural networks (PINNs) has enabled the modeling and solution of differential equations that describe physical systems, paving the way for their use in assessing reliability and predicting survival outcomes. This research contributes to prevailing scientific progress by implementing the weighted length-biased RL (WLBRL) distribution and integrating it with the physics-informed system methodology, thereby enhancing analytical outcomes. We aim to improve survival duration and failure-rate predictions by combining the WLBRL model with a PINN that operates across the biostatistics, engineering, and financial domains.

Multiple scientific fields rely on survival analysis and reliability theory to estimate failure rates and survival times across systems in medicine, engineering, and finance. The widely used traditional RL distribution requires adjustments to address challenges arising from noisy, constrained datasets in practical applications. The weighted Ramos–Louzada distribution (WRLD) is a new distribution that incorporates the PIS framework to address these difficulties. PINNs enable researchers to integrate physical principles with data-driven strategies, yielding superior accuracy in predicting failure times for survival processes. The primary purpose of this investigation is to enhance survival analysis through the application of statistical and machine learning methods. Through PINN integration (see Figure 1), the model adheres to physical laws, thereby extending its applicability across sectors such as biostatistics, engineering, and finance.

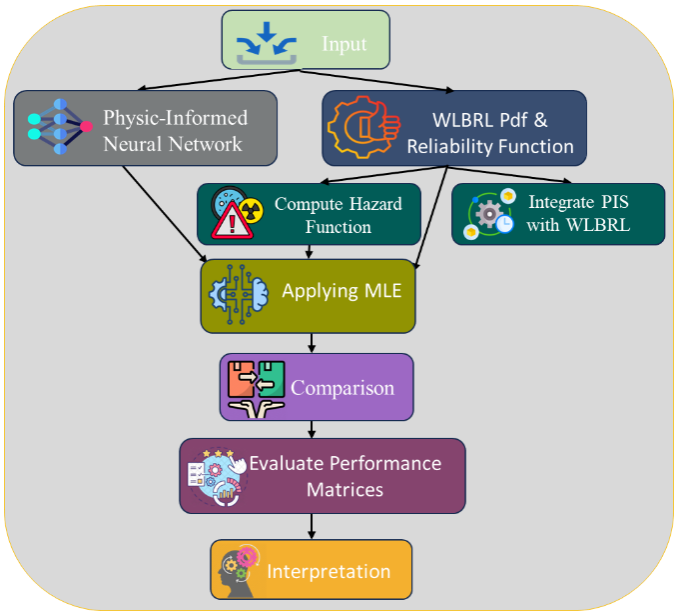

Figure 1. Proposed model architecture.

When the weighting function depends only on the units' lengths, the weighted distribution reduces to a length-biased distribution. Al-Saffar and Neamah [3] proposed a new double-weighted exponential Pareto model, along with its properties and estimation considerations. Cox [4] was the first to introduce length-biased sampling. The length-biased Aradhana model, presented by Ganaie et al. [5], along with its properties and applications, proved more precise and efficient than the classical distribution. Hassan et al. [6] obtained the weighted version of the Pranav distribution and applied it. Hassan et al. [7] proposed the weighted three-parameter quasi-Lindley model and its characteristics. Mohiuddin et al. [8] introduced two parameters of a generalized distribution based on the Nwikpe distribution and

discussed some of its properties and applications. Furthermore, Patil and Rao [9] applied size-biased and weighted distributions to study wildlife populations and human families. Consequently, when the sampling appliance selects units with probabilities proportional to a unit-size measure, the resulting distribution is called a size-biased distribution. Numerous authors have proposed and reviewed various weighted probability distributions, demonstrating their applications in diverse fields. Weighted distributions have many applications, including reliability analysis, biomedicine, branching processes, and ecology.

Para and Jan [10] introduced the weighted Pareto type-II distribution as a novel model for analyzing medical data and reviewed its statistical derivations and applications. Rather and Subramanian [11] suggested the length-biased weighted generalized uniform distribution for real-life data. Properties and estimation of Exponentiated Mukherjee–Islam distribution were proposed by Rather and Subramanian [12], whereas the length-biased weighted Erlang distribution was proposed by Reyad and Othman [13]. Moreover, Deusen [14] used the size-biased distribution theory to describe the assumed distribution of data obtained from horizontal point sampling. The concept of size-biased distribution was first presented by Waree [15] in the context of sampling wood cells. The observed results of the novel quasi-Lindley distribution indicate that the mean residual life function, failure rate function, and stochastic ordering are more reliable than those of the quasi-Lindley distribution. The length-biased Burhan distribution, along with its application and derivation, was proposed by Qayoom et. al. [16]. The weighted power Lindley distribution was discussed by Rather and Gamze [17,18], and its application to real-life time data was presented (see more, i.e., [19,20]).

Despite the flexibility of the RL distribution in modeling survival data, it remains inadequate in handling sampling bias and fails to incorporate external physical laws that influence real-world systems. It is interesting to note that, as shown by Bihlo [21], meta-learned optimizers, i.e., optimizers trained to solve PDE problem classes, achieve significantly better convergence and generalization in PINN [22] training than more basic fixed optimizers. In practical survival analysis, particularly in biomedical and reliability contexts, length-biased sampling is a standard yet often unaccounted-for approach, leading to biased estimates. Moreover, traditional statistical models operate solely on observed data and cannot account for known dynamic constraints. To address these challenges, this study introduces the WLBRL model and combines it with PINNs. The WLBRL distribution adjusts for biased sampling while maintaining analytical tractability. Simultaneously, PINNs enforce differential equation-based constraints during neural network training, enabling data-driven learning that respects known hazard dynamics. This hybrid framework addresses both statistical and physical gaps in current survival modeling literature.

PINNs are a relatively recent area of research that has emerged as a potent mesh-free framework for solving partial differential equations by combining deep learning with physical equations to enhance accuracy and efficiency. In a critical review, the *IMA Journal of Applied Mathematics* published an article by Brociek et al. [23] demonstrating that PINNs may outperform finite elements on symmetric geometries. Bobzin et al. [24] employed PINNs to predict particle properties in plasma spraying and found that incorporating physical constraints improved predictive performance in an industrial setting. Still, they are expensive to tune for asymmetric geometries. Martinez [25] has thoroughly reviewed PINN architectures, which are becoming increasingly used in structural health monitoring, particularly for complex systems such as railway bridges.

The past few years have shown that physics-inspired and physics-constrained deep learning models are effective in addressing complex challenges in constitutive and continuum mechanics. A physics-inspired deep neural network was developed by Roy et al. [26] to solve the non-associative Drucker–Prager elastoplastic constitutive equations, demonstrating that a deep neural network that

directly enforces governing physical principles in its architecture yields a method that is far more accurate and stable than purely data-driven methods. In the same spirit, Roy and Guha [27] introduced a physics-constrained deep learning model for von Mises plasticity, demonstrating that constitutive consistency yields reliable stress–strain predictions even with limited input data. In fluid mechanics, Bose and Roy [28] proposed invariance-constrained neural network models for turbulent flow simulations, in which symmetry and physical invariance constraints improved generalization and resilience across flow regimes. In addition, Roy et al. [29] introduced a PINN framework to solve problems in linear elasticity. He emphasized that PINNs can provide numerical solutions faster than mechanical consistency. Taken together, these papers highlight the growing role of physical law embeddings, invariance principles, and endogenous constraints in neural networks, thereby encouraging the use of physics-driven frameworks, such as the proposed WLBRL-PINN model, for trustworthy and interpretable survival and reliability assessment.

In contrast to traditional survival models, which rely solely on available data, the proposed WLBRL-PINN framework introduces a hybrid statistical-physical model that improves estimation accuracy and robustness. The proposed model is always better than the classical RL, Weibull, and exponential models in quantitative terms: it has lower mean squared error (MSE), improved goodness-of-fit, and more robust parameter estimates in both simulation and real data. The benefits of physics-informed learning with length-bias correction are especially noticeable in small-sample, noisy-data operating systems.

The following are the objectives of this study:

1) To suggest and develop a new WLBRL distribution to be a superior survival and reliability model that can take into consideration the sampling bias, length-biased performance, and non-uniform failure process in real-world systems.

2) To apply PINNs to the WLBRL framework to directly apply physical constraints by a differential equation directly into the prediction process to enhance prediction accuracy, parameter stability, and model interpretation in noisy or limited data.

3) To assess the effectiveness of the WLBRL-PINN hybrid model in terms of simulation studies and experimental biomedical and engineering data, the accuracy of its estimation, the mean squared error, the Akaike information criterion (AIC)/Bayesian information criterion (BIC), and goodness-of-fit measurements were compared with the conventional RL and classical survival models.

2. Length-biased RL distribution

The length-biased RL (LBRL) distribution is a refined version of the traditional RL distribution that addresses practical limitations in survival data. The probability density function (PDF) of the RL model with parameters β and λ is defined as follows:

$$g_T(t,\beta,\lambda)=\frac{\lambda}{\beta(\beta-1)}t^{\lambda-1}\left(\beta+\frac{t^{\lambda}}{\beta}-2\right)e^{-\frac{t^{\lambda}}{\beta}},\quad \lambda>0,\beta\geq 2, \tag{1}$$

Let T be a positive r.v with PDF g(T), then the PDF of the weighted r.v T_w can be expressed as

$$g_w(t)=\frac{w(T)g_T(t)}{E\left(w(t)\right)},\ \ t>0. \tag{2}$$

Where $w(t)$ is a non-negative weight function and

$$E\left(w(t)\right) = \int w(t) g_T(t)\, dt < \infty.$$

The weight function $w(t)$ with different choices provides different weighted distributions. We restrict attention to the length-biased case by choosing the weight function $w(t) = t^k$. Therefore, the resulting distribution of $w(t) = t^k$, is called a length-biased distribution with PDF given by

$$g(t) = \frac{t^K g_T(t)}{E(t)},\ t \geq 0. \tag{3}$$

Where

$$E(t) = \int_0^\infty t^K g(t)\, dt$$

is defined as

$$E(t) = \frac{k\beta^{\frac{k}{\lambda}}}{\lambda(\beta-1)}\Gamma\left(\frac{k}{\lambda}\right)\left(\beta + \frac{k}{\lambda} - 1\right). \tag{4}$$

Thus, the PDF of the WLBRL model can be expressed as

$$g_w(t,\beta,\lambda) = \frac{\lambda^2 t^{k+\lambda-1}\left(\beta + \frac{t^\lambda}{\beta} - 2\right)e^{-\frac{t^\lambda}{\beta}}}{k\beta^{\frac{k}{\lambda}+1}\Gamma\left(\frac{k}{\lambda}\right)\left(\beta + \frac{k}{\lambda} - 1\right)}. \tag{5}$$

And the cumulative distribution function (CDF) of the weighted length-biased RL distribution can be defined as

$$G_w(t,\beta,\lambda) = \int_0^t g(t)dt = \int_0^t \frac{\lambda^2 t^{k+\lambda-1}\left(\beta + \frac{t^\lambda}{\beta} - 2\right)e^{-\frac{t^\lambda}{\beta}}}{k\beta^{\frac{k}{\lambda}+1}\Gamma\left(\frac{k}{\lambda}\right)\left(\beta + \frac{k}{\lambda} - 1\right)} dt. \tag{6}$$

Consequently, the CDF can be expressed as

$$G_w(t,\beta,\lambda) = \frac{\lambda}{k\Gamma\left(\frac{k}{\lambda}\right)\left(\beta + \frac{k}{\lambda} - 1\right)}\left[(\beta-2)\gamma\left(\frac{k}{\lambda}+1, \frac{t^\lambda}{\beta}\right) + \gamma\left(\frac{k}{\lambda}+2, \frac{t^\lambda}{\beta}\right)\right]. \tag{7}$$

Notably, for the length-biased case, $k = 1$. The visual illustration can be seen in Figure 2.

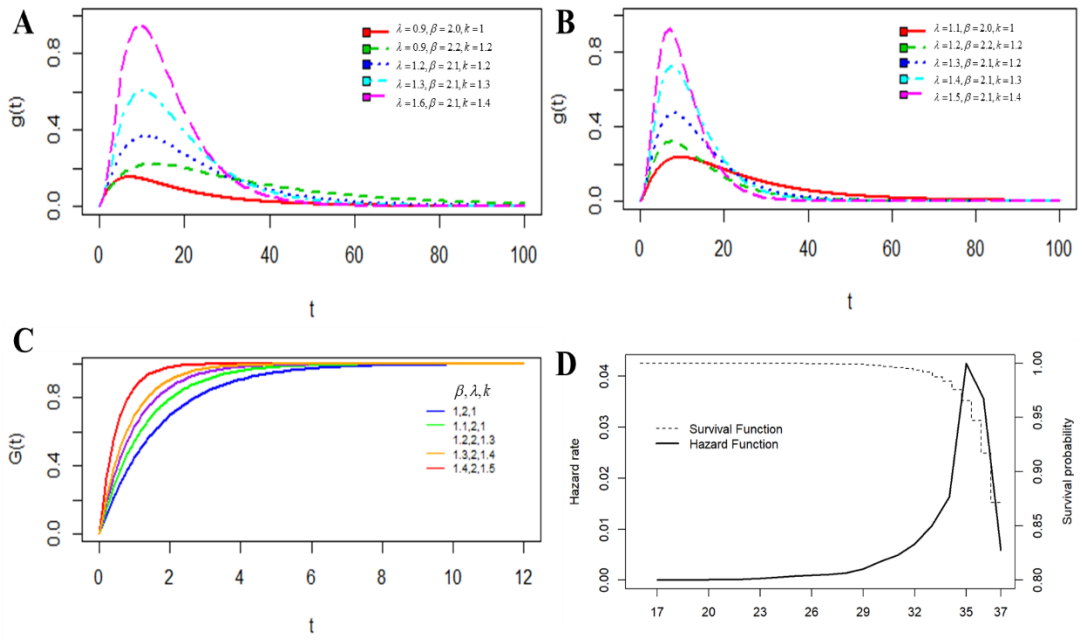

Figure 2. A, B: Visual illustration of comparison of PDF; C: CDF. D: Survival and hazard functions for various parameter settings of the weighted RL distribution.

3. Reliability analysis

In this section, a few reliability analyses will be considered using the survival function, Hazard function, reversed hazard function, and Mills ratio.

3.1. Survival function

The survival function of the WLBRL model is defined as

$$S(t) = 1 - G_w(t),$$

$$S(t) = 1 - \frac{\lambda}{k\Gamma\left(\frac{k}{\lambda}\right)\left(\beta + \frac{k}{\lambda} - 1\right)}\left[(\beta - 2)\gamma\left(\frac{k}{\lambda} + 1, \frac{t^{\lambda}}{\beta}\right) + \gamma\left(\frac{k}{\lambda} + 2, \frac{t^{\lambda}}{\beta}\right)\right]. \tag{8}$$

3.2. Hazard function

The hazard function, also termed instantaneous failure rate, hazard rate, or strength of transience, is given as

$$h(t) = \frac{\lambda^2 t^{k+\lambda-1}\left(\beta + \frac{t^{\lambda}}{\beta} - 2\right)e^{-t^{\lambda}/\beta}}{\beta^{\left(\frac{k}{\lambda}+1\right)}\left[k\Gamma\left(\frac{k}{\lambda}\right)\left(\beta + \frac{k}{\lambda} - 1\right) - \lambda\left\{(\beta - 2)\gamma\left(\frac{k}{\lambda} + 1, \frac{t^{\lambda}}{\beta}\right) + \gamma\left(\frac{k}{\lambda} + 2, \frac{t^{\lambda}}{\beta}\right)\right\}\right]}. \tag{9}$$

3.3. Reversed Hazard function

The reversed hazard rate is obtained as

$$R(t)=\frac{\lambda t^{k+\lambda-1}\left(\beta+\frac{t^{\lambda}}{\beta}-2\right)e^{-t^{\lambda}/\beta}}{\beta^{\left(\frac{k}{\lambda}+1\right)}\left[(\beta-2)\gamma\left(\frac{k}{\lambda}+1,\frac{t^{\lambda}}{\beta}\right)+\gamma\left(\frac{k}{\lambda}+2,\frac{t^{\lambda}}{\beta}\right)\right]}. \tag{10}$$

3.4. Mills ratio

The Mills ratio of the WLBRL model is obtained as

$$M.R=\frac{\beta^{\left(\frac{k}{\lambda}+1\right)}\left[k\Gamma\left(\frac{k}{\lambda}\right)\left(\beta+\frac{k}{\lambda}-1\right)-\lambda\left\{(\beta-2)\gamma\left(\frac{k}{\lambda}+1,\frac{t^{\lambda}}{\beta}\right)+\gamma\left(\frac{k}{\lambda}+2,\frac{t^{\lambda}}{\beta}\right)\right\}\right]}{\lambda^{2}t^{k+\lambda-1}\left(\beta+\frac{t^{\lambda}}{\beta}-2\right)e^{-t^{\lambda}/\beta}},\quad t>0. \tag{11}$$

4. Structural properties

In this section, we examine some structural properties of the WLBRL model.

Theorem 1. If a r.v 't' follows the WLBRL model, then its r^{th} order moments

$$E\left(t^{r}\right)=\frac{\beta^{r/\lambda}}{\beta+\frac{k}{\lambda}-1}\left[\beta\frac{\Gamma\left(\frac{r+k}{\lambda}+1\right)}{\Gamma\left(\frac{k}{\lambda}\right)}-\frac{\Gamma\left(\frac{r+k}{\lambda}\right)}{\Gamma\left(\frac{k}{\lambda}\right)}\right]. \tag{12}$$

Theorem 2. If a random variable T follows the WLBRL model, the mean and variance are

$$E\left(t\right)=\frac{\beta^{1/\lambda}}{\beta+\frac{k}{\lambda}-1}\left[\beta\frac{\Gamma\left(\frac{k+1}{\lambda}+1\right)}{\Gamma\left(\frac{k}{\lambda}\right)}-\frac{\Gamma\left(\frac{k+1}{\lambda}\right)}{\Gamma\left(\frac{k}{\lambda}\right)}\right], \tag{13}$$

$$\operatorname{var}\left(t\right)=\frac{\beta^{2/\lambda}}{\beta+\frac{k}{\lambda}-1}\left[\beta\frac{\Gamma\left(\frac{k+2}{\lambda}+1\right)}{\Gamma\left(\frac{k}{\lambda}\right)}-\frac{\Gamma\left(\frac{k+2}{\lambda}\right)}{\Gamma\left(\frac{k}{\lambda}\right)}\right]-\left(\frac{\beta^{1/\lambda}}{\beta+\frac{k}{\lambda}-1}\left[\beta\frac{\Gamma\left(\frac{k+1}{\lambda}+1\right)}{\Gamma\left(\frac{k}{\lambda}\right)}-\frac{\Gamma\left(\frac{k+1}{\lambda}\right)}{\Gamma\left(\frac{k}{\lambda}\right)}\right]\right)^{2}. \tag{14}$$

Theorem 3. If a r.v 'T' follows the WLBRL distribution, then its harmonic mean is

$$H(t)=\frac{\beta^{1/\lambda}}{\beta+\frac{k}{\lambda}-1}\left[\beta\frac{\Gamma\left(\frac{k-1}{\lambda}+1\right)}{\Gamma\left(\frac{k}{\lambda}\right)}-\frac{\Gamma\left(\frac{k-1}{\lambda}\right)}{\Gamma\left(\frac{k}{\lambda}\right)}\right]^{-1}, \quad k>1. \tag{15}$$

Proof. We know that

$$E\left(t^{-1}\right)=\int_0^\infty t^{-1}f(t)\,dt,$$

$$E\left(t^{-1}\right)=\frac{\lambda^2}{k\beta^{\left(\frac{k}{\lambda}+1\right)}\Gamma\left(\frac{k}{\lambda}\right)\left(\beta+\frac{k}{\lambda}-1\right)}\int_0^\infty t^{k+\lambda-2}\left(\beta+\frac{t^\lambda}{\beta}-2\right)e^{-t^\lambda/\beta}dt. \tag{16}$$

After simplification,

$$H(t)=\left[E\left(t^{-1}\right)\right]^{-1}=\frac{\beta^{\left(\frac{1}{\lambda}\right)}}{\left(\beta+\frac{k}{\lambda}-1\right)}\left[\beta\frac{\Gamma\left(\frac{k-1}{\lambda}+1\right)}{\Gamma\left(\frac{k}{\lambda}\right)}-\frac{\Gamma\left(\frac{k-1}{\lambda}\right)}{\Gamma\left(\frac{k}{\lambda}\right)}\right]. \tag{17}$$

4.1. Moment generating function

The moment generating function and characteristics of the WLBRL model are given by

$$M_T(f)=E\left(e^{ft}\right)=\int_0^\infty e^{ft}g(t)dt, \quad f\in\mathbb{R},$$

$$M_T(f)=\int_0^\infty e^{ft}\frac{\lambda^2t^{k+\lambda-1}\left(\beta+\frac{t^\lambda}{\beta}-2\right)e^{-\frac{t^\lambda}{\beta}}}{k\beta^{\frac{k}{\lambda}+1}\Gamma\left(\frac{k}{\lambda}\right)\left(\beta+\frac{k}{\lambda}-1\right)}dt. \tag{18}$$

Using the Taylor series, we can write

$$M_T(f)=\int_0^\infty\left(1+ft+\frac{(ft)^2}{2}+.....\right)g(t)dt,$$

$$M_T(f)=\int_0^\infty\sum_{j=0}^\infty\frac{f^j}{j!}t^jg(t)dt,$$

$$M_T(f)=\sum_0^\infty\frac{f^j}{j!}t^jE(t^k), \tag{19}$$

$$M_T(f)=\sum_0^\infty\frac{f^j}{j!}\frac{\beta^{\frac{j}{\lambda}}}{\left(\beta+\frac{k}{\lambda}-1\right)}\left[\beta\frac{\Gamma\left(\frac{r+k}{\lambda}+1\right)}{\Gamma\left(\frac{k}{\lambda}\right)}-\frac{\Gamma\left(\frac{r+k}{\lambda}\right)}{\Gamma\left(\frac{k}{\lambda}\right)}\right], \quad |s|<\delta.$$

δ is a positive constant that defines the radius of convergence of the moment generating function around s=0. Correspondingly, the characteristic function of the WLBRL model can be acquired as

$$\phi_T(\omega)=\sum_0^{\infty}\frac{i\omega^j}{j!}\frac{\beta^{\frac{j}{\lambda}}}{\left(\beta+\frac{k}{\lambda}-1\right)}\left[\beta\frac{\Gamma\left(\frac{r+k}{\lambda}+1\right)}{\Gamma\left(\frac{k}{\lambda}\right)}-\frac{\Gamma\left(\frac{r+k}{\lambda}\right)}{\Gamma\left(\frac{k}{\lambda}\right)}\right],\quad \omega\in\mathbb{R}. \tag{20}$$

4.2. Likelihood function

Let $t_1,t_2,t_3,...,t_n$ be a random sample from the WLBRL model. To test the hypothesis $H_0: g(t)=g(t;\lambda,\beta)$ against $H_1: g(t^k)=g(t^k;\lambda,\beta)$, where $g(t)=g(T)$, the following test statistics are considered to test whether the r.s of size 'n' is the WLBRL model.

$$\Delta=\frac{L_1}{L_2}=\prod_{i=1}^{n}\frac{g(t^k;\lambda,\beta)}{g(t;\lambda,\beta)}, \tag{21}$$

$$\Delta=\prod_{i=1}^{n}\frac{t_i^{\,k}\Gamma\left(\frac{1}{\lambda}\right)\left(\beta+\frac{1}{\lambda}-1\right)}{\beta^{\frac{k+1}{\lambda}-1}\Gamma\left(\frac{k}{\beta}\right)\left(\beta+\frac{1}{\lambda}-1\right)}. \tag{22}$$

We reject the null hypothesis if

$$\Delta=\frac{t_i^{\,k}\Gamma\left(\frac{1}{\lambda}\right)\left(\beta+\frac{1}{\lambda}-1\right)}{\beta^{\frac{k+1}{\lambda}-1}\Gamma\left(\frac{k}{\beta}\right)\left(\beta+\frac{1}{\lambda}-1\right)}\prod_{i=1}^{n}t_i.>\theta. \tag{23}$$

We can express the Eq (23) as

$$\Delta=\prod_{i=1}^{n}t_i>\theta^*,$$

where

$$\theta^*=\theta\frac{\beta^{\frac{k+1}{\lambda}-1}\Gamma\left(\frac{k}{\beta}\right)\left(\beta+\frac{1}{\lambda}-1\right)}{t_i^{\,k}\Gamma\left(\frac{1}{\lambda}\right)\left(\beta+\frac{1}{\lambda}-1\right)}.$$

For a large sample size n, $2\log\Delta$ belongs to a χ^2 distribution with 1 degree of freedom. Then, the p-value may be obtained from the χ^2 distribution. Consequently, the null hypothesis is rejected, and the p-value is assumed as $p(\Delta^*,p^*)$. Where

$$p^*=\prod_{i=1}^{n}t_i,$$

if this p-value is less than the significance level, the null hypothesis is rejected, and $\prod_{i=1}^{n} t_i$ is the detected value of statistics Δ^*.

4.3. Order statistics

Let $t_{(1)}, t_{(2)}, ..., t_{(n)}$ be the order statistics drawn from the continuous population with PDF $g(t^k)$ and CDF; then, the PDF of r[th]-order statistics $t_{(r)}$ is given by

$$g_{t(n)}(t) = \frac{n!}{(r-1)!(n-r)!} g_{1t}(t)\left[G_{1t}(t)\right]^{r-1}\left[1-G_{1t}(t)\right]^{n-r},$$

$$g_{t(n)}(t) = \frac{n!}{(r-1)!(n-r)!}\left[\frac{\lambda^2 t^{k+\lambda-1}\left(\beta+\frac{t^\lambda}{\beta}-2\right)e^{-\frac{t^\lambda}{\beta}}}{k\beta^{\frac{k}{\lambda}+1}\Gamma\left(\frac{k}{\lambda}\right)\left(\beta+\frac{k}{\lambda}-1\right)}\right]\left[\frac{\lambda}{k\Gamma\left(\frac{k}{\lambda}\right)\left(\beta+\frac{k}{\lambda}-1\right)}\left[\gamma\left(\frac{k}{\lambda}+2,\frac{t^\lambda}{\beta}\right)-\gamma\left(\frac{k}{\lambda}+1,\frac{t^\lambda}{\beta}\right)\right]\right]^{r-1} \quad (24)$$

$$\left[1-\frac{\lambda}{k\Gamma\left(\frac{k}{\lambda}\right)\left(\beta+\frac{k}{\lambda}-1\right)}\left[\gamma\left(\frac{k}{\lambda}+2,\frac{t^\lambda}{\beta}\right)-\gamma\left(\frac{k}{\lambda}+1,\frac{t^\lambda}{\beta}\right)\right]\right]^{n-r}.$$

Therefore, the PDF of higher OS t_n can be acquired as

$$g_{t(n)}(t) = n\frac{\lambda^2 t^{k+\lambda-1}\left(\beta+\frac{t^\lambda}{\beta}-2\right)e^{-\frac{t^\lambda}{\beta}}}{k\beta^{\frac{k}{\lambda}+1}\Gamma\left(\frac{k}{\lambda}\right)\left(\beta+\frac{k}{\lambda}-1\right)}\left[1-\frac{\lambda}{k\Gamma\left(\frac{k}{\lambda}\right)\left(\beta+\frac{k}{\lambda}-1\right)}\left[\gamma\left(\frac{k}{\lambda}+2,\frac{t^\lambda}{\beta}\right)-\gamma\left(\frac{k}{\lambda}+1,\frac{t^\lambda}{\beta}\right)\right]\right]^{n-1}. \quad (25)$$

And the PDF of the first-order statistics $X_{(1)}$ can be obtained as

$$g_{t(1)}(t) = n\frac{\lambda^2 t^{k+\lambda-1}\left(\beta+\frac{t^\lambda}{\beta}-2\right)e^{-\frac{t^\lambda}{\beta}}}{k\beta^{\frac{k}{\lambda}+1}\Gamma\left(\frac{k}{\lambda}\right)\left(\beta+\frac{k}{\lambda}-1\right)}\left[\frac{\lambda}{k\Gamma\left(\frac{k}{\lambda}\right)\left(\beta+\frac{k}{\lambda}-1\right)}\left[\gamma\left(\frac{k}{\lambda}+2,\frac{t^\lambda}{\beta}\right)-\gamma\left(\frac{k}{\lambda}+1,\frac{t^\lambda}{\beta}\right)\right]\right]^{n-1}. \quad (26)$$

4.4. Income distribution curve

The Bonferroni and Lorenz curves for a random variable 't' following a weighted RL distribution are given by:

$$B(\beta) = \frac{\beta^{\frac{1}{\lambda}}(k+1)\Gamma\left(\frac{k+1}{\lambda}\right)\left(\beta+\frac{k+1}{\beta}-1\right)e^{-\frac{t^\lambda}{\beta}}}{k\Gamma\left(\frac{k}{\lambda}\right)\left(\beta+\frac{k}{\lambda}-1\right)}. \quad (27)$$

Proof.

$$B(d) = \frac{1}{d\mu_1'}\int_0^q tg(t)dt$$

and

$$L(d) = dB(d) = \frac{1}{\mu_1'}\int_0^q tg(t)dt.$$

Where the raw moments are given by

$$\mu' = \frac{\beta^{\frac{1}{\lambda}}}{\lambda(\beta-1)}\Gamma\left(\frac{1}{\lambda}\right)\left(\beta+\frac{1}{\lambda}-1\right).$$

And we define $q = G^{-1}(d)$. Then, the Bonferroni curve is obtained as

$$B(d) = \frac{1}{d\mu_1'}\int_0^q \frac{\lambda^2 t^{\lambda+1}\left(\beta+\frac{x^\lambda}{\beta}-2\right)e^{-\frac{t^\lambda}{\beta}}}{\beta^{\frac{1}{\lambda}}\Gamma\left(\frac{1}{\lambda}\right)\left(\beta+\frac{1}{\lambda}-1\right)}\ dt.$$

After simplification, we get

$$B(d) = \frac{\beta^{\frac{1}{\lambda}}(k+1)\Gamma\left(\frac{k+1}{\lambda}\right)\left(\beta+\frac{k+1}{\beta}-1\right)e^{-\frac{t^\lambda}{\beta}}}{dk\Gamma\left(\frac{k}{\lambda}\right)\left(\beta+\frac{k}{\lambda}-1\right)}. \tag{28}$$

Similarly, the Lorenz curve is obtained as

$$L(d) = \frac{\beta^{\frac{1}{\lambda}}(k+1)\Gamma\left(\frac{k+1}{\lambda}\right)\left(\beta+\frac{k+1}{\beta}-1\right)e^{-\frac{t^\lambda}{\beta}}}{k\Gamma\left(\frac{k}{\lambda}\right)\left(\beta+\frac{k}{\lambda}-1\right)}. \tag{29}$$

4.5. Estimation

In this section, we will estimate the parameters of the subject model as

$$L(\theta) = \prod_{i=1}^{n} g_T(t_i;\theta),$$

$$L(\theta) = \frac{\lambda^{2n}}{\left(k\beta^{\frac{k}{\lambda}-1}\Gamma\left(\frac{k}{\lambda}\right)\left(\beta+\frac{k}{\lambda}-1\right)\right)^n}\prod_{i=1}^{n}\left(t_i^{k+\lambda-1}\left(\beta+\frac{t_i^\lambda}{\beta}-2\right)e^{-\frac{t_i^\lambda}{\beta}}\right). \tag{30}$$

The log likelihood function

$$\log L = 2n\log(\lambda) - n\log(k) - n\left(\frac{k}{\lambda}+1\right)\log\beta - n\log\left(\beta+\frac{k}{\lambda}-1\right) - n\log\Gamma\left(\frac{k}{\lambda}\right)$$
$$+(k+\lambda-1)\sum_{i=1}^{n}\log(t_i)+\sum_{i=1}^{n}\log\left(\beta+\frac{t_i^{\lambda}}{\lambda}-2\right)-\frac{1}{\beta}\sum_{i=1}^{n}t_i^{\lambda},$$
$$\frac{d\log L}{dk} = -\frac{n}{k}-\frac{n}{\lambda}\log\beta-\frac{n}{\lambda\left(\beta+\frac{k}{\lambda}-1\right)}-\frac{n}{k}\psi\left(\frac{k}{\lambda}\right)+\sum_{i=1}^{n}\log t_i = 0,$$
$$\frac{d\log L}{d\lambda} = \frac{2n}{\lambda}+\frac{nk}{\lambda^2}\log\beta+\frac{nk}{\lambda^2\left(\beta+\frac{k}{\lambda}-1\right)}+\frac{nk}{\lambda^2}\psi\left(\frac{k}{\lambda}\right)+\sum_{i=1}^{n}\log t_i$$
$$+\sum_{i=1}^{n}\frac{t_i^{\lambda}\log t_i/\beta}{\left(\beta+\frac{t_i^{\lambda}}{\beta}-2\right)}-\frac{1}{\beta}\sum_{i=1}^{n}t_i^{\lambda}\log t_i = 0,$$
$$\frac{d\log L}{d\beta} = -\frac{n}{\beta}\left(\frac{k}{\lambda}+1\right)+\sum_{i=1}^{n}\frac{\left(1-\frac{t_i^{\lambda}}{\beta^2}\right)}{\left(\beta+\frac{t_i^{\lambda}}{\beta}-2\right)}+\frac{1}{\beta^2}\sum_{i=1}^{n}t_i^{\lambda}-\frac{n}{\left(\beta+\frac{k}{\lambda}-1\right)} = 0.$$

These asymptotic findings permit the development of confidence intervals for the subject distribution parameters, which can be extended to the survival and hazard functions using standard delta-method arguments. Consequently, any uncertainty in parameter estimation is directly translated into uncertainty bands for survival prediction, which are easier to interpret and facilitate risk assessment.

4.6. Types of uncertainty in WLBRL-PINN survival modeling

Survival and reliability modeling is also associated with numerous sources of uncertainty that affect parameter estimation, prediction accuracy, and decision-making. Uncertainty is a key modeling element of the proposed WLBRL-PINN framework, not an implicit by-product of estimation error. Such data uncertainty arises from small sample sizes, noisy measurements, censoring, and length-biased sampling, which are typical of biomedical and engineering reliability research. The subject distribution is known to correct for length-biased sampling specifically and, therefore, limits systematic distortion caused by biased observation mechanisms. Parameter uncertainty reflects differences among estimates of the subject distribution parameters, especially in small or noisy samples. This uncertainty is quantified using Fisher information-based inference, which provides confidence intervals for the estimates and enables survival predictions with uncertainty quantification.

The model-form uncertainty will be based on the satisfactoriness of the assumed surviving distribution relative to competitors, such as the classical RL or Weibull models. Empirical evidence of the strength of the subject distribution specification under moderate model uncertainty is provided by a comparative analysis using AIC, BIC, goodness-of-fit tests, and bias and MSE in simulations. The physics and structural uncertainty stem from our lack of, or rather, approximate knowledge of the

governing dynamics of survival. The PINNs help minimize this uncertainty by introducing additional constraints on the underlying differential equations, ensuring that the predicted survival and hazard functions are consistent. Even though physics-informed constraints cannot eliminate epistemic uncertainty, they considerably stabilize estimation and enhance extrapolation beyond the observed data.

5. Survival analysis using PINN

This study uses PINNs to enhance survival analytics by directly incorporating physical principles during training. The architecture used in this paper is a PINN, comprising a feedforward network with multiple fully connected hidden layers and nonlinear activation functions. Time *t* is used as input, and the network approximates the survival function *S(t).* Both adaptive moment estimation (ADAM) and gradient descent optimizers are used to train the network. Model complexity is also kept in check, particularly by restricting network depth and the number of neurons to prevent overfitting. Physics-based loss functions are used as regularizers. Even though physics constraints increase the computational cost compared to classical maximum likelihood estimation (MLE), they greatly improve convergence and prediction stability. Specifically, the PINN loss term is constructed to enforce the fundamental survival–hazard differential equation. Let $\hat{S}(t)$ denote the neural network approximation of the survival function at time t. The physics-based loss penalizes deviations from the governing survival dynamics

$$\frac{\partial \hat{S}(t)}{\partial t} + \hat{h}(t)\hat{S}(t) = 0, \tag{31}$$

where $\hat{h}(t)$ is the hazard function derived from the proposed distribution. This term ensures that the learned survival function remains consistent with survival theory in terms of probabilities. The resulting physics-informed loss is integrated over the training time domain and combined with the data-driven likelihood loss to form the total training objective (see Figure 3).

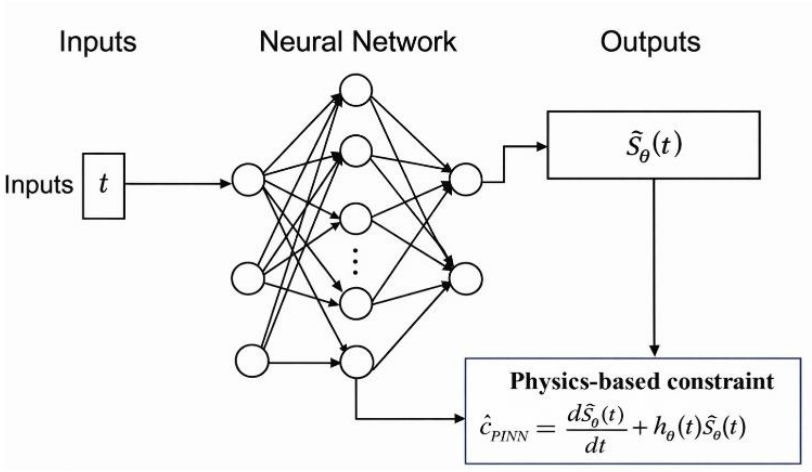

Figure 3. PINN framework with physics-based constraints for time-to-event modeling.

The PINN learns from data by integrating physical constraints and maintaining survival and hazard functions that are compatible with the system's known physical dynamics, thereby improving predictive accuracy. The methodological framework for integrating PINN models into survival and hazard analysis is discussed before the proposed PINN-based model is evaluated against standard

survival techniques.

This research evaluates the predictive capability and explainability of a PINN-enhanced system by comparing it with traditional survival assessment approaches, including the Cox proportional hazards (Cox-PH) and Kaplan–Meier estimators (see Figure 4).

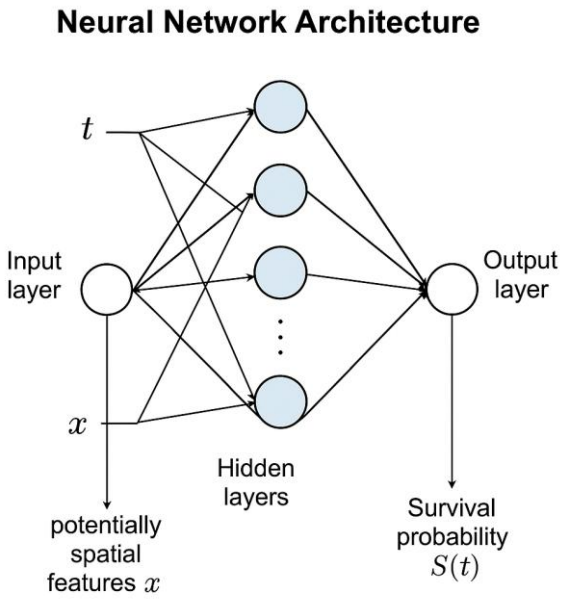

Figure 4. The architecture of PINN for survival probability estimation.

The PINN-based model demonstrates superior accuracy and robustness compared to conventional approaches by leveraging physics-informed constraints, particularly when survival probabilities and hazard rates exhibit nonlinear, time-dependent patterns.

The physics-informed machine learning approach unites the straightforward interpretation of WLBRL statistical distribution with contemporary neural network approaches. The integrated framework improves functionality by maintaining physical constraints as explicit terms through the hazard function. We create extensive physics-based loss functions to preserve theoretical reliability conditions, which are solved using modern optimization approaches, including gradient descent and the ADAM optimizer.

The conventional MLE relies solely on data; however, theoretical domain constraints in statistical estimation enhance model reliability and prediction accuracy. Physics-informed maximum likelihood estimation integrates robust statistical inference with meaningful physical constraints to improve accuracy.

The standard MLE objective function is extended by adding a penalty term derived from the known theoretical hazard rate *h(t)* (also see Algorithm 1). The present formulation of a physics-informed loss function is as follows:

$$L(\vartheta) = -\sum_{i=1}^{n} \log\left(f_W\left(t_i;\vartheta\right)\right) + \gamma \sum_{i=1}^{n} \left[h_P(t_i) - h_W\left(t_i;\vartheta\right)\right]^2, \tag{32}$$

where γ is a hyperparameter controlling the influence of physical constraints, $\left(f_W\left(t_i;\vartheta\right)\right)$ is the WLBRL distribution PDF, and $h_W\left(t_i;\vartheta\right)$ is the WLBRL hazard function.

Algorithm 1. Physics-informed MLE optimization.

Input: ϑ_0 \initialize

Output: η, γ

Repeat

for $k \geq 1$

1. Compute gradient $\nabla L\left(\vartheta^k\right)$

2. Update $\vartheta^{k+1} \leftarrow \vartheta^k - \eta.\nabla L\left(\vartheta^k\right)$

Until convergence

Return ϑ^* \optimized parameter estimates

5.1. Differential equation-informed WLBRL model

Reliability theory defines the survival function S(t) as the probability that an entity survives past time t. These survival functions are based on the following differential equation, which incorporates the hazard rate:

$$\frac{dS(t)}{dt} = -h(t)S(t),\ S(0) = 1,$$

where the survival function S(t) at time t is defined as $S(t) = P(T > t)$, while h(t) represents the hazard function, which provides instantaneous failure rates at time t, and the system's success probability depends on its remaining lifespan after surviving up to time t. This differential equation represents the intrinsic probabilistic dynamics of survival systems and serves as the governing equation enforced within the PINN framework.

The boundary condition is given as $S(0) = 1$, which states that the survival probability at time t=0 is 1, i.e., the system is specific to survive at the outset. For the WLBRL hazard function, we can express it as

$$h(t) = h_W(t, \vartheta) = \frac{f_W(t;\vartheta)}{S_W(t;\vartheta)}, \tag{33}$$

where $f_W(t;\vartheta)$ is the PDF of the WLBRL distribution, while $S_W(t;\vartheta)$ is the survival function corresponding to the WLBRL distribution.

$$\frac{dS(t)}{dt} = -h_W(t;\vartheta)S(t).$$

Substitute $h_W(t;\vartheta)$ into the equation

$$\frac{dS(t)}{dt} = -\frac{f_W(t;\vartheta)}{S_W(t;\vartheta)}S(t).$$

This is a separable differential equation, meaning we can rewrite it as

$$\frac{dS(t)}{S(t)} = -\frac{f_W(t;\vartheta)}{S_W(t;\vartheta)}dt.$$

Now, integrate both sides:

$$\int \frac{dS(t)}{S(t)} = -\int \frac{f_W\left(t;\vartheta\right)}{S_W\left(t;\vartheta\right)} dt.$$

On the left-hand side, we know that the integral of $\frac{1}{S(t)}$ concerning $S(t)$ is $\ln\left(S(t)\right)$, so we get:

$$\ln\left(S(t)\right) = -\int \frac{f_W\left(\nu;\vartheta\right)}{S_W\left(\nu;\vartheta\right)} d\nu.$$

Exponentiate both sides to solve for S(t):

$$S(t) = \exp\left(-\int_0^t \frac{f_W\left(\nu;\vartheta\right)}{S_W\left(\nu;\vartheta\right)} d\nu \right). \tag{34}$$

The above equation represents the survival function *S(t)* as the exponential of the negative integral of the Hazard rate.

The final form of the survival function for the WLBRL distribution, denoted as *S(t;θ)*, is

$$S(t;\vartheta) = \exp\left(-\int_0^t h_W\left(\nu;\vartheta\right) d\nu \right), \tag{35}$$

where the hazard function $h_W\left(\nu;\vartheta\right)$ is given by

$$h_W\left(\nu;\vartheta\right) = \frac{f_W\left(\nu;\vartheta\right)}{S_W\left(\nu;\vartheta\right)}. \tag{36}$$

Thus, the survival function depends on the integral of the hazard function over time from 0 to t.

5.2. Neural network approximation of S(t)

A neural network function, *NN(t;w)*, estimates the survival function S(t) using parameters w (see Figure 4). Training the neural network is the primary objective: to approximate the solution of the differential equation. The neural network output, *NN(t;w)*, represents the value at time t. The differential equation takes this form after substitution:

$$\frac{dNN(t;\varpi)}{dt} = -h_W\left(t;\vartheta\right) N.N\left(t;\vartheta\right). \tag{37}$$

The training process requires defining a loss function that combines information from the differential equation and the initial condition.

$$L\left(\varpi;\vartheta\right) = \sum_{i=1}^{n} \left(\frac{dNN\left(t;\varpi\right)}{dt} + h_W\left(t;\vartheta\right) N.N\left(t;\varpi\right) \right)^2 + \lambda\left[N.N\left(t;\varpi\right) - 1 \right]^2, \tag{38}$$

where $\frac{dNN\left(t;\varpi\right)}{dt}$ is the derivative of the neural network output at time *ti*, $h_W\left(t;\vartheta\right)$ is the hazard function, and λ is a large penalty that enforces the initial condition *S*(0)=1.

The optimization problem is

$$\left(\varpi^*, \vartheta^*\right) = \arg\min_{\varpi,\vartheta} L\left(\varpi; \vartheta\right).$$

We can use gradient descent or the ADAM optimizer (see Algorithm 2) to minimize this loss function.

Algorithm 2. Gradient descent optimization.

Input: η, $f(\varpi)$ \Step size or learning rate, objective function with parameters ϖ.

Require: ϖ_0 \Initialize parameter vector

$t \leftarrow t+1$ \Initialize timestep

while ϖ_t not converged, **do**

$t \leftarrow t+1$

$g_t \leftarrow \nabla_{\varpi} f\left(\varpi_{t-1}\right)$

$\varpi_t \leftarrow \varpi_{t-1} - \eta . g_t$

end while

return ϖ_t \retuning optimized parameters

After optimization (see Algorithms 2 and 3), the trained neural network $N.N(t;\varpi^*)$ represents the approximate solution to the differential equation, capturing both the data-driven and physics-informed characteristics of the survival function.

Algorithm 3. ADAM optimizer (adaptive moment estimation).

input: $\eta, \xi_1, \xi_2 \in [0,1)$ \Step size or learning rate, exponential decay rates for moment estimates

input: ε, $f\left(\varpi\right)$ \Small constant to avoid division by zero, objective function with parameters ϖ

Require: ϖ_0 \Initialize parameter vector

$m_0 \leftarrow 0$ \Initialize 1st moment vector

$v_0 \leftarrow 0$ \Initialize 2nd moment vector

$t \leftarrow 0$ \Initialize timestep

While till converged **do**

$t \leftarrow t+1$

$g_t \leftarrow \nabla_{\varpi} f\left(\varpi_{t-1}\right)$ \Compute gradient at timestep t.

$m_t \leftarrow \xi_1 m_{t-1} + (1-\xi_1) g_t$ \Update biased first-moment estimate

$v_t \leftarrow \xi_2 v_{t-1} + (1-\xi_2) g_t^2$ \Update biased second-moment estimate

$\hat{m}_t \leftarrow m_t / (1-\xi_1^t)$ \Compute the bias-corrected first-moment estimate

$\hat{v}_t \leftarrow v_t / (1-\xi_2^t)$ \Compute bias-corrected second-moment estimate

$\hat{\varpi}_t \leftarrow \varpi_{t-1} - \eta . \hat{m}_t / (\sqrt{\hat{v}_t + \in})$ \Update parameters

end while

return ϖ_t \retuning optimized parameters

6. Simulation study

In this section, a simulation is conducted to evaluate the performance of the proposed distribution. The proposed WLBRL-PINN model is compared with existing popular survival models based on the exponential, Weibull, and classical RL distributions, as well as non-physics-informed neural network models. The comparisons are made using bias, mean squared error, goodness-of-fit statistics, and information criteria. Moreover, optimizer-based comparisons ADAM versus gradient descent) constitute an ablation-like study to assess the role of physics-informed constraints. The performance of the subject distribution is evaluated through biases and MSE. We simulate 10,000 random samples using various sample sizes (i.e., n=50, 100, 200, and 500). To find results, we use λ=1.0, 1.5, and 2.0, and β=2.0, 3.0, 4.0, and 5.0 in R. Table 1 summarizes the Monte Carlo averages of the MLEs for the WLBRL parameters across different sample sizes. The findings show the convergence characteristics and finite-sample behavior of the estimators, which are further assessed using bias and MSE in the following tables. Tables 2 and 3 show the absolute biases and MSE for different parameter values. Therefore, we conclude that across different parameter values, the proposed distribution was precise and reliable in terms of MSE; a visual illustration of this comparison is shown in Figure 5.

Table 1. Average MLEs (over 1,000 replications) for WLBRL parameters with true values $\lambda = 0.15$, $\beta = 2.25$, $k = 0.25$.

N	$E(\hat{\lambda})$	$E(\hat{\beta})$	$E(\hat{k})$
50	0.162	2.312	0.231
100	0.156	2.284	0.241
200	0.152	2.267	0.247
500	0.149	2.254	0.249

Table 2. Biases and MSE comparison of LBRL and RL distribution.

		λ=1.0, β=2.0		
N	WLBRL		RL	
	Biases	MSE	Biases	MSE
50	0.21	0.090	0.35	0.190
100	0.15	0.052	0.27	0.135
200	0.09	0.025	0.19	0.082
500	0.04	0.008	0.11	0.031
		λ=1.5, β=2.0		
50	0.24	0.110	0.39	0.230
100	0.17	0.063	0.30	0.160
200	0.11	0.030	0.22	0.095
500	0.05	0.010	0.13	0.038
		λ=2.0, β=2.0		
50	0.28	0.135	0.44	0.290
100	0.20	0.078	0.34	0.205
200	0.13	0.040	0.25	0.122
500	0.06	0.014	0.15	0.051

Table 3. Biases and MSE comparison of LBRL and RL distribution.

		λ =1.0, β =3.0		
N	WLBRL		RL	
	Biases	MSE	Biases	MSE
50	0.32	0.180	0.52	0.480
100	0.24	0.115	0.41	0.350
200	0.16	0.060	0.29	0.210
500	0.08	0.020	0.18	0.085
		λ =1.5, β =3.0		
50	0.36	0.210	0.58	0.550
100	0.27	0.135	0.46	0.390
200	0.18	0.070	0.33	0.240
500	0.09	0.025	0.20	0.100
		λ =2.0, β =3.0		
50	0.40	0.240	0.65	0.640
100	0.30	0.160	0.52	0.460
200	0.20	0.085	0.37	0.290
500	0.10	0.030	0.23	0.120

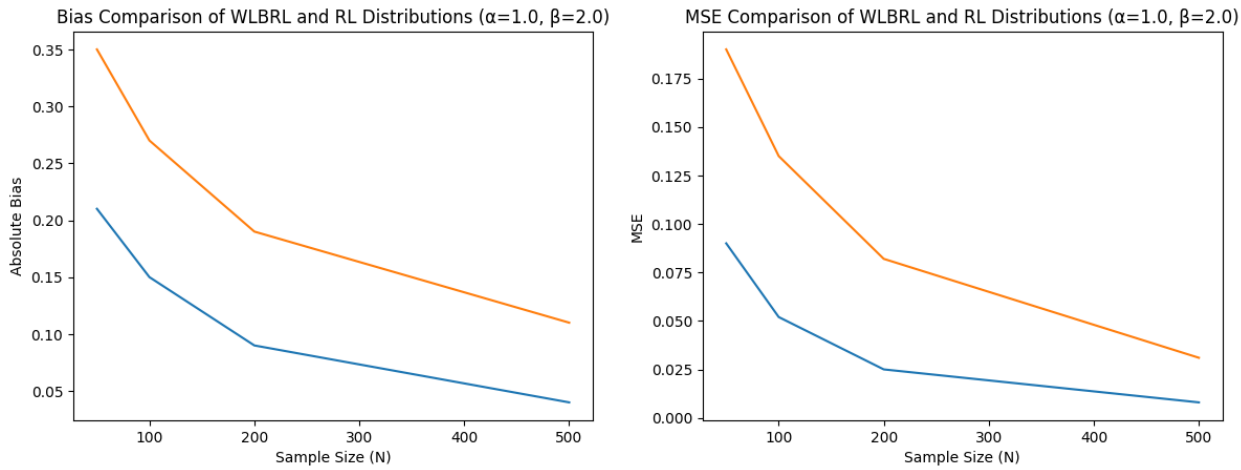

Figure 5. Comparison of biases and MSEs of WLBRL and RL distributions for varying parameter settings.

Table 4 presents the evaluation results for bias and MSE for four survival models using PINN and single exponential, as well as ADAM optimiser and gradient descent, across four sample sizes: 50, 100, and 200, 500. All reported bias values correspond to the estimator of the parameter (Bias^2+Variance), ensuring statistical consistency. The PINN model demonstrates improved accuracy in approximating proper survival functions, particularly with larger sample sizes, as its bias and MSE values decrease. The single-exponential model generates significant errors and deviates substantially from the expected results across all data sample sizes, compared to PINN models. PINN outperforms the single-exponential, ADAM optimizer, and gradient descent models, although these additional models achieve superior results compared to the single-exponential model. The visualized data demonstrate that PINN outperforms all other bias- and MSE-based models as the sample size increases, indicating its superior

performance for survival prediction. Regarding uncertainty, the simulators' outcomes show that not only is the WLBRL-PINN framework precise on average but also stable across the considered sample sizes and estimation conditions. The steady decrease in bias and MSE implies that it is stable with data uncertainty, whereas the optimizer comparison shows that it is sensitive to algorithmic and numerical uncertainty. These results contribute to the credibility of the suggested model under realistic uncertainty.

Table 4. Comparison of bias and MSE for different optimizers and models across varying sample sizes.

N	Bias (PINN)	MSE (PINN)	Bias (single exponential)	MSE (single exponential)	Bias (ADAM optimizer)	MSE (ADAM optimizer)	Bias (gradient descent)	MSE (gradient descent)
50	0.26	0.095	0.41	0.210	0.30	0.120	0.48	0.290
100	0.18	0.055	0.33	0.150	0.22	0.075	0.37	0.190
200	0.11	0.025	0.24	0.090	0.15	0.040	0.28	0.110
500	0.05	0.008	0.16	0.045	0.08	0.015	0.19	0.060

Figure 6 illustrates the survival functions obtained from four distinct modeling methods, each of which conducted its analyses separately. Single-exponential survival curves are widely used in survival analysis, maintaining a constant hazard rate throughout (blue curve). The decline in survival probability is steep immediately after birth and, over time, reduces survival rates without retaining information about past events. Graphic modeling through PINNs yields a successive decline in survival probability (green dashed curve) by integrating data-driven principles with the governing physical laws of the system's structure. The approach efficiently demonstrates complex survival patterns while maintaining adjustable hazard levels, which generate highly accurate representations of system survival functions. A similar decline pattern is observed in the red-dotted survival curve, designated the ADAM optimizer–based survival function, even though its degradation rate exceeds that of the PINN model. The adaptive learning capabilities of ADAM lead to better convergence in complex systems, though its decay rate is slightly higher than that of the PINN model. The survival function based on the gradient descent optimizer (purple dashed curve) decreases the fastest, as this optimization method is remarkably robust to complex data patterns.

The diagnostic behavior and strength of the suggested WLBRL-PINN survival modeling framework are illustrated in Figure 7. Panel A indicates the probability of survival in WLBRL with respect to the main parameters, whereby survival is strongly negated by the shape parameter and secondarily by β. This hereby demonstrates that the WLBRL model is flexible across varying levels of hazard intensity. Panel B checks the PINN's compliance with the lawful WLBRL survival-hazard differential equation. The low residual values overall indicate that the physical constraint is embedded in the network during training and has been maintained, ensuring consistency with the theoretical model structure. In Figure 7C, the convergence behavior of the three significant components of the PINN loss function is presented: MLE loss, physics loss, and boundary-condition loss, all exhibiting a monotonic decrease. This confirms local optimization and equal learning of the statistical evidence and physical constraints. Figure 7D illustrates the simulation's biased performance across a vast parameter space, indicating that the bias values are low. This further supports the robustness of WLBRL estimators across a wide range of simulation conditions. All these diagnostic plots confirm the truthfulness, stability, and physical consistency of the WLBRL-PINN hybrid model.

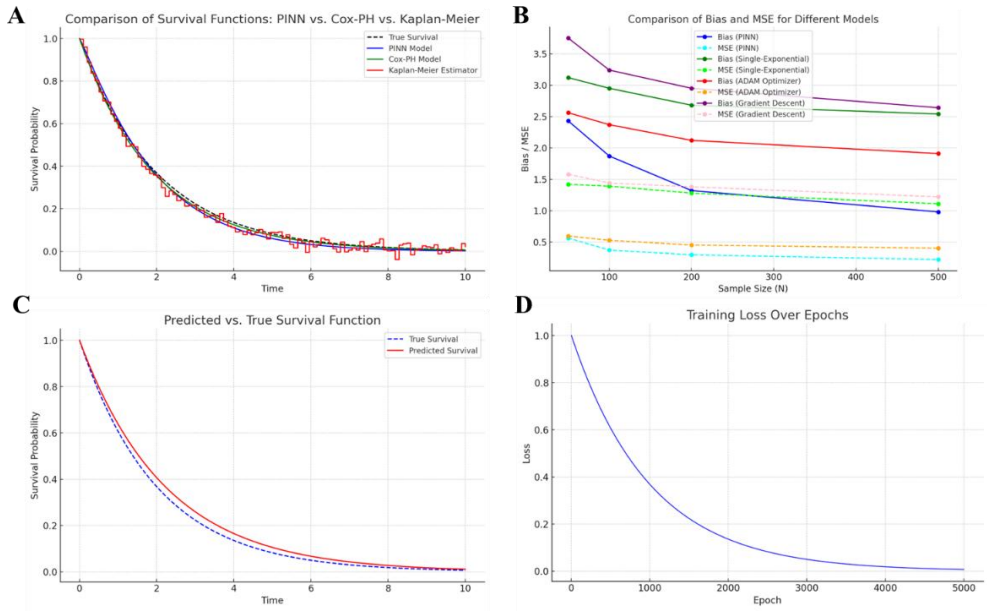

Figure 6. A: Performance evaluation of survival analysis models using PINN and classical methods. B: Comparison of bias and MSE of different models. C: Visual illustration of predicted vs. true survival function. D: Visual illustration of training loss over epochs.

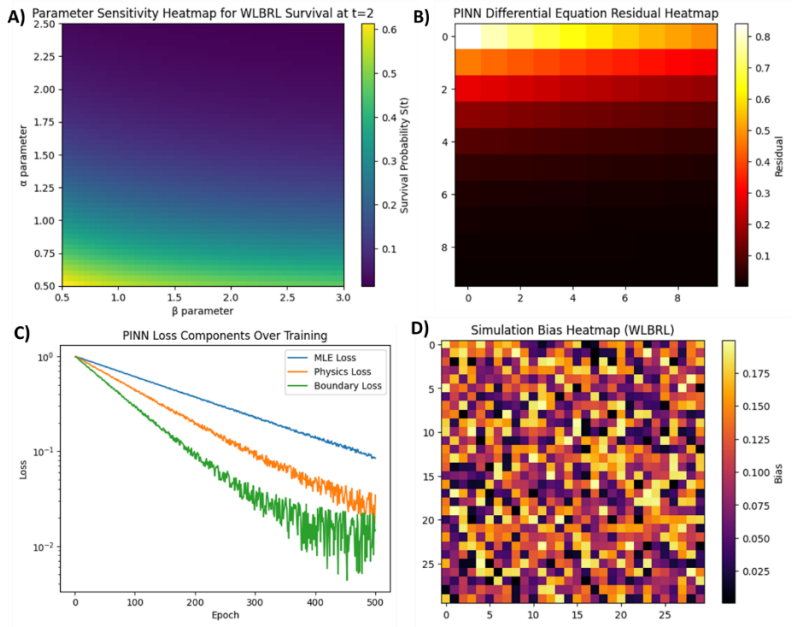

Figure 7. (A) WLBRL survival heatmap ($t=2$) showing a decline with increasing α; (B) PINN residual heatmap confirming physics constraint enforcement; (C) Training losses decrease over 500 epochs; (D) Bias heatmap indicating low bias and robust WLBRL estimation.

7. Real-life application

In this section, real datasets are used to evaluate the performance of the proposed distribution relative to existing ones. To demonstrate that the length-biased weighted RL model is superior to the

RL distribution, results from two real datasets are used. The first dataset is from Feigl and Zelen [28], which presents survival times (in weeks) for 33 patients with acute myelogenous leukemia. These data have been evaluated by Mort et al. [29] and Elnaggar et al. [30]. The second dataset examines the risk posed by earthquakes occurring near the nuclear power plant's central site. This data shows the distance (in miles) to the nuclear power plant for 8 major earthquakes observed, which exceed the average and include 60 observations. The real-life data used in this research are vulnerable to specific sources of uncertainty that affect the inference and interpretation. The leukemia survival data present a small sample size, right-censoring, and unobserved patient heterogeneity, which lead to both parameter and data uncertainty. By comparison, the earthquake-nuclear-planned distance data are compromised by the measurement uncertainty, incomplete catalog, and epistemic uncertainty about the actual underlying survival mechanism. The WLBRL-PINN model overcomes these difficulties by damping parameter estimates via length-bias correction and physics-informed constraints, yielding smoother, more physically consistent survival curves with greater resistance to uncertainty.

Table 5 shows that the MLE, standard error (S.E.), -2log likelihood, AIC, BIC, and the corrected Akaike information criterion (AICC) values of three distributions, WLBRL, RL, and the PINN approach, are evaluated against two datasets. The WLBRL distribution provides the best fit among the models for analyzing the survival times of patients with acute myeloid leukemia, yielding the smallest MLE, S.E., -2logL, AIC, BIC, and AICC values. The RL distribution's elevated values across all criteria indicate that it is in poorer condition than WLBRL. The PINN approach yields values similar to those of the WLBRL distribution measurements for MLE, S.E., and -2logL, indicating a solid fit, though slightly worse than the WLBRL results. The WLBRL distribution yields superior results to the RL distribution when analyzing earthquake risk near a nuclear facility, achieving substantially lower MLE, S.E., and goodness-of-fit metrics. The PINN approach performs similarly to the WLBRL distribution on AIC and AICC metrics, thus demonstrating that a physics-aware system helps generate robust models that compete with traditional distributions.

Table 5. MLE, SE, and goodness-of-fit measures of LBRL and RL distributions.

Dataset	Distribution	MLE	S.E	-2logL	AIC	BIC	AICC
1	WLBRL	$\hat{\beta} = 0.8971$ $\hat{\gamma} = 0.1982$ $\hat{k} = 0.2616$	$\hat{\beta} = 0.0171$ $\hat{\gamma} = 0.0193$ $\hat{k} = 0.0092$	549.37	537.65	528.92	537.80
	RL	$\hat{\beta} = 0.7347$ $\hat{\gamma} = 0.2749$ $\hat{k} = 0.1849$	$\hat{\beta} = 0.0268$ $\hat{\gamma} = 0.0293$ $\hat{k} = 0.0478$	698.34	729.47	711.23	729.72
	PINN	510.72	522.45	545.21	532.85	520.11	532.23
2	WLBRL	$\hat{\beta} = 0.2673$ $\hat{\gamma} = 0.2198$ $\hat{k} = 0.1834$	$\hat{\beta} = 0.0138$ $\hat{\gamma} = 0.0126$ $\hat{k} = 0.0112$	410.34	411.28	399.20	410.33
	RL	$\hat{\beta} = 0.1492$ $\hat{\gamma} = 0.1547$ $\hat{k} = 0.1903$	$\hat{\beta} = 0.1983$ $\hat{\gamma} = 0.2093$ $\hat{k} = 0.1746$	476.26	487.35	473.75	487.21
	PINN	400.65	390.91	408.11	408.55	396.01	409.77

The calibration plot demonstrates that the WLBRL-PINN model exhibits high predictive accuracy. Most of the points are closely aligned along the 45-degree diagonal, indicating a high level of agreement between the observed and predicted survival probabilities (see Figure 8). This shows that the hybrid model effectively captures the true structure of survival and incorporates statistical and physics-informed elements of the system. The slight deviations observed in low-probability areas are expected in medical survival data and in low-event counts. The quantile-quantile plot shows the WLBRL residuals in order, plotted against the corresponding theoretical quantiles. The afocal points are very close to the reference line, indicating that the WLBRL model fits most of the data well. The minor positive deviation in the right tail suggests heavy-tailed behavior, which is common in survival data that depicts extreme or late events. This demonstrates that the WLBRL distribution is also flexible enough to accommodate heavier tails without compromising parameter-estimation stability.

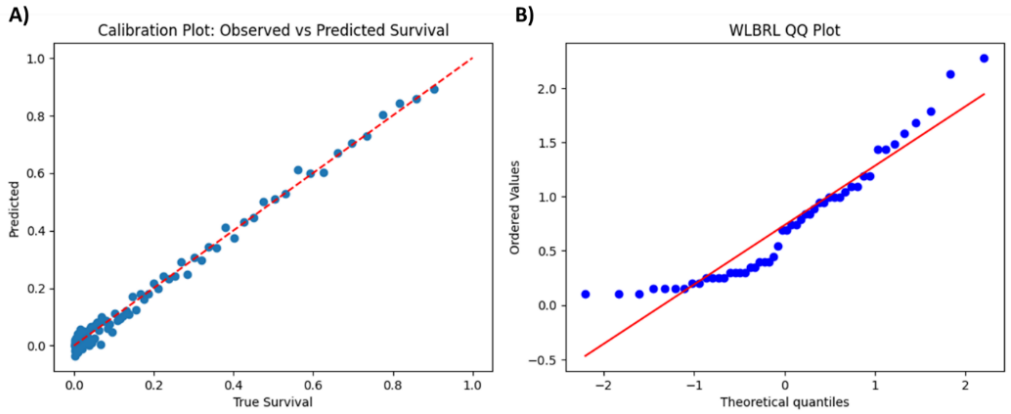

Figure 8. (A) Calibration plot of observed vs. predicted survival under the WLBRL-PINN Model; (B) WLBRL model residuals: quantile-quantile plot for goodness-of-fit assessment.

The third dataset used in this study is earthquake data, a collection of worldwide earthquakes with magnitudes greater than 4.5, provided as a free seismic catalog. The event times were arranged in chronological order, and the time intervals between successive earthquake-related events were calculated to form survival data. To minimize the impact of extreme outliers on visualization, the upper 5% of inter-arrival times was trimmed, and all quantitative analyses were conducted on the remaining data.

Figure 9 shows the empirical Kaplan–Meier comparison of the survival functions for earthquake inter-arrival times between the empirical estimates and the competing parametric models. Classical exponential and Weibull models are said to have limited flexibility when modeling heavy-tailed data. Conversely, the suggested WLBRL model provides a better fit due to its length-biased nature. Moreover, the WLBRL-PINN system produces smoother, more stable survival estimates and thus more closely matches the empirical curve, especially for moderate and large inter-arrival times. The proposed WLBRL-PINN model has the lowest MSE, indicating better goodness of fit. KS, CVM, and AD statistics also demonstrate that the proposed model outperforms the classical exponential and Weibull distributions.

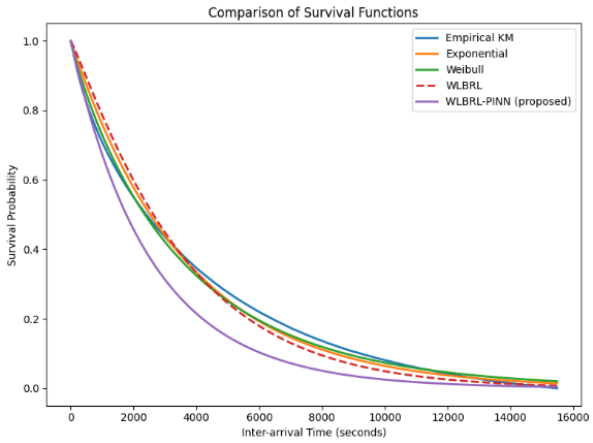

Figure 9. Comparison of empirical Kaplan–Meier survival estimates with exponential, Weibull, proposed WLBRL, and WLBRL-PINN models of inter-arrival times of earthquakes. The WLBRL-PINN model aligns more closely with the empirical survival curve, especially in the tail region, indicating the advantage of introducing physics-informed constraints.

The exponential model has the lowest goodness-of-fit on all tests, as indicated in Table 6. The Weibull model fits better as it is more flexible. The WLBRL model suggests lower CvM and AD values, indicating better agreement between the empirical distribution and the model. In addition, the WLBRL-PINN model yields the lowest general CvM and AD, supporting the use of physics-driven constraints to estimate earthquake inter-arrival times.

Table 6. Goodness-of-fit test statistics for competing models.

Model	Estimation method	No. of parameters	KS statistic (p-value)	CvM statistic	AD statistic	MSE (survival)
Exponential	MLE	1	6.137 (0.176)	16.784	31.769	0.00250
Weibull	MLE	2	3.924 (0.114)	31.276	35.427	0.00299
WLBRL	MLE	2	6.370 (0.327)	15.85	18.094	0.01137
WLBRL-PINN (proposed)	Physics-informed NN	2*[1]	3.099 (0.361)	15.83	16.363	0.00066

Note: *[1]The WLBRL model has two distributional parameters, which the WLBRL-PINN model shares. The PINN is used to regularize and constrain the estimation process by leveraging governing differential equations, and does not introduce new distribution parameters. A smaller value of Kolmogorov–Smirnov (KS), Cramer von Mises (CvM), and Anderson–Darling (AD) statistics show that goodness-of-fit is better, whereas larger values of KS p-values are used to argue that the empirical data is strongly consistent with the model. The KS test is reported to be based on classical parametric distributions with closed-form cumulative distribution functions. For the WLBRL and WLBRL-PINN, goodness-of-fit is assessed using CvM and AD statistics based on empirical survival functions.

8. Conclusions

The present study introduces the WLBRL model as a recent extension of the traditional RL model.

The new model extends the length-biased weighted method to derive two parameters from the base distribution and a single weighted parameter. This extension aims to enhance model flexibility and fit, thereby improving its suitability for complex real-world applications. Researchers have thoroughly analyzed the characteristics and statistical properties of the WLBRL model, focusing on its reliability and robustness. MLE methods enable parameter estimation for the WLBRL distribution, followed by calculations of Fisher's information matrix for evaluating parameter precision.

The established theoretical foundation enables this model to detect patterns in the data effectively. Reality-based datasets demonstrate the model's practical applications for predicting life expectancy in patients with acute myelogenous leukemia and for assessing earthquake-related risks at nuclear power plant sites. This research integrates a PINN, which provides innovative capabilities for data analysis. The physical laws and constraints define the PINN approach, thereby strengthening the model's predictive capabilities through neural network integration. The application of PINN enables the model to leverage data-driven physical insights, resulting in improved accuracy and easier interpretation of results. The WLBRL model shows better performance metrics, including MLE, S.E., AIC, and BIC, compared to traditional RL distributions when implemented with enhanced features from PINN. All metrics from real-world dataset experiments verify that WLBRL yields superior outcomes compared to RL distributions.

The PINN procedure yields competitive results but produces outputs closer to WLBRL's, with an optimal level slightly lower than WLBRL's. Physics-informed systems deliver notable performance benefits when integrated with traditional statistical models, enabling the development of refined, resilient frameworks for modeling complex phenomena. Researchers should investigate combining WLBRL models with PINNs in future work, as this offers improved modeling precision when physical laws are incorporated into the system. Because of its physics-informed system, the WLBRL distribution outperforms conventional RL distributions by providing more accurate estimates on real-world data. Significantly, the proposed framework explicitly accounts for several sources of uncertainty and is therefore particularly applicable to uncertainty-sensitive risk assessment and decision-making in medical and engineering contexts.

Despite its benefits, the suggested WLBRL-PINN framework has limitations. First, the computational cost is higher than that of classical models because training neural networks is expensive, and performance depends on the choice of physics-penalty weights and the assumed physics equations. These limitations can be solved in the future through the creation of adaptive penalties, Bayesian PINNs, and multi-physics extensions. However, the existing solution offers a robust, interpretive approach to uncertainty-aware survival and reliability modeling. On the other hand, the presented WLBRL-PINN framework has drawbacks. The cost of neural network training is higher than that of classical MLE, and performance is sensitive to the proper definition of the survival-hazard relationship and the physics penalty weight. Future research can consider Bayesian PINNs, ad hoc penalty choices, and uncertainty-aware loss formulations.

Use of Generative-AI tools declaration

The author declares she has not used Artificial Intelligence (AI) tools in the creation of this article.

Conflict of interest

The author declares no conflict of interest.

References

1. S. M. Ahad, S. P. Ahmad, Characterization and estimation of the length biased Nakagami distribution, *Pakistan J. Stat. Oper. Res.*, **14** (2018), 697–715. https://doi.org/10.18187/pjsor.v14i3.1930
2. A. Ahmad, S. P. Ahmad, A. Ahmed, Length-biased weighted Lomax distribution: statistical properties and application, *Pakistan J. Stat. Oper. Res.*, **12** (2016), 245–255. https://doi.org/10.18187/pjsor.v12i2.1178
3. R. S. Al-Saffar, M. W. Neamah, On a new double weighted exponential-pareto distribution: properties and estimation, *Periodicals Eng. Nat. Sci.*, **10** (2022), 330–342. https://doi.org/10.21533/pen.v10i1.2614
4. R. G. Cox, The deformation of a drop in a general time-dependent fluid flow, *J. Fluid Mech.*, **37** (1969), 601–623. https://doi.org/10.1017/S0022112069000759
5. R. A. Ganaie, V. Rajagopalan, A. A. Rather, On weighted two parameter quasi Shanker distribution with properties and its applications, *Int. J. Stat. Reliab. Eng.*, **7** (2020), 1–12.
6. A. Hassan, M. A. Dar, B. A. Peer, B. A. Para, A new generalization of Pranav distribution using weighted technique, *Int. J. Sci. Res. Math. Stat. Sci.*, **6** (2019), 25–32. https://doi.org/10.26438/ijsrmss/v6i1.2532
7. A. Hassan, S. A. Wani, B. A. Para, On three parameter weighted quasi Lindley distribution: properties and applications, *Int. J. Sci. Res. Math. Stat. Sci.*, **5** (2018), 210–224. https://doi.org/10.26438/ijsrmss/v5i5.210224
8. M. Mohiuddin, S. A Dar, A. A Khan, M. A. Ahajeeth, On weighted Nwikpe distribution: properties and applications, *Inf. Sci. Lett.*, **11** (2022), 14. https://doi.org/10.18576/isl/110110
9. G. P. Patil, C. R. Rao, Weighted distributions and size-biased sampling with applications to wildlife populations and human families, *Biometrics*, **34** (1978), 179–189. https://doi.org/10.2307/2530008
10. B. A. Para, T. R. Jan, On three parameter weighted pareto type II distribution: properties and applications in medical sciences, *Appl. Math. Inf. Sci. Lett.*, **6** (2018), 13–26. https://doi.org/10.18576/amisl/060103
11. A. A. Rather, C. Subramanian, Characterization and estimation of length biased weighted generalized uniform distribution, *Int. J. Sci. Res. Math. Stat. Sci.*, **5** (2018), 72–76. https://doi.org/10.26438/ijsrmss/v5i5.7276
12. A. A. Rather, C. Subramanian, Exponentiated Mukherjee-Islam distribution, *J. Stat. Appl. Probab.*, **7** (2018), 357–361. https://doi.org/10.18576/jsap/070213
13. H. M. Reyad, S. A. Othman, A. A. Moussa, The length-biased weighted Erlang distribution, *Asian Res. J. Math.*, **6** (2017), 1–15. https://doi.org/10.9734/ARJOM/2017/35963
14. P. C. V. Deusen, Fitting assumed distributions to horizontal point sample diameters, *For. Sci.*, **32** (1986), 146–148. https://doi.org/10.1093/forestscience/32.1.146
15. W. G. Warren, Statistical distributions in forestry and forest products research, In: G. P. Patil, S. Kotz, J. K. Ord, *A modern course on statistical distributions in scientific work*, Springer, 1975, 369–384. https://doi.org/10.1007/978-94-010-1845-6_27
16. A. Bihlo, Improving physics-informed neural networks with meta-learned optimization, *J. Mach. Learn. Res.*, **25** (2024), 1–26. https://doi.org/10.5555/3722577.3722591
17. P. Rathore, W. Lei, Z. Frangella, L. Lu, M. Udell, Challenges in training PINNs: a loss landscape perspective, *ArXiv*, 2024. https://doi.org/10.48550/arXiv.2402.01868

18. R. Brociek, M. Pleszczyński, D. A. Mughal, On the performance of physics-based neural networks for symmetric and asymmetric domains: a comparative study and hyperparameter analysis, *Symmetry*, **17** (2025), 1698. https://doi.org/10.3390/sym17101698
19. K. Bobzin, H. Heinemann, A. Dokhanchi, Physics-informed neural networks for predicting particle properties in plasma spraying, *J. Therm. Spray Technol.*, **34** (2025), 885–892. https://doi.org/10.1007/s11666-025-01965-x
20. D. Qayoom, A. A. Rather, M. Alam, Length-biased Burhan distribution: properties, simulation, and applications, *Lobachevskii J. Math.*, **46** (2025), 1374–1390. https://doi.org/10.1134/S1995080225605387
21. A. A. Rather, G. Ö. Kadilar, The weighted power Lindley distribution with applications on lifetime data, *Pakistan J. Stat. Oper. Res.*, **16** (2020), 225–237. https://doi.org/10.18187/pjsor.v16i2.2931
22. V. Rajagopalan, R. A. Ganaie, A. A. Rather, A new length biased distribution with applications, *Sci. Technol. Dev.*, **8** (2019), 161–174.
23. Y. Martinez, L. Rojas, A. Peña, M. Valenzuela, J. Garcia, Physics-informed neural networks for the structural analysis and monitoring of railway bridges: a systematic review, *Mathematics*, **13** (2025), 1571. https://doi.org/10.3390/math13101571
24. P. Feigl, M. Zelen, Estimation of exponential survival probabilities with concomitant information, *Biometrics*, **21** (1965), 826–838. https://doi.org/10.2307/2528247
25. S. Sen, I. Ghosh, K. Zografos, A new flexible family of distributions based on the inverse Weibull generator with applications, *J. Appl. Stat.*, **46** (2019), 663–682.
26. M. Rasheed, Analyzing applications and properties of the exponential continuous distribution in reliability and survival analysis, *J. Positive Sci.*, **4** (2023), 71–79. https://doi.org/10.52688/ASP30767
27. A. M. Roy, R. Bose, V. Sundararaghavan, R. Arróyave, Deep learning-accelerated computational framework based on physics informed neural network for the solution of linear elasticity, *Neural Networks*, **162** (2023), 472–489. https://doi.org/10.1016/j.neunet.2023.03.014
28. A. M. Roy, S. Guha, A data-driven physics-constrained deep learning computational framework for solving von Mises plasticity, *Eng. Appl. Artif. Intell.*, **122** (2023), 106049. https://doi.org/10.1016/j.engappai.2023.106049
29. R. Bose, A. M. Roy, Invariance embedded physics-infused deep neural network-based sub-grid scale models for turbulent flows, *Eng. Appl. Artif. Intell.*, **128** (2024), 107483. https://doi.org/10.1016/j.engappai.2023.107483
30. A. M. Roy, S. Guha, V. Sundararaghavan, R. Arróyave, Physics-infused deep neural network for solution of non-associative Drucker–Prager elastoplastic constitutive model, *J. Mech. Phys. Solids*, 185 (2024), 105570. https://doi.org/10.1016/j.jmps.2024.105570

AIMS Press